

Long-Term Immobilization in Elderly Females Causes a Specific Pattern of Cortical Bone and Osteocyte Deterioration Different From Postmenopausal Osteoporosis

Tim Rolvien,^{1,2†} Petar Milovanovic,^{1,3†} Felix N Schmidt,¹ Simon von Kroge,¹ Eva M Wölfel,¹ Matthias Krause,^{1,4} Birgit Wulff,⁵ Klaus Püschel,⁵ Robert O Ritchie,⁶ Michael Amling,¹  and Björn Busse¹ 

¹Department of Osteology and Biomechanics, University Medical Center Hamburg-Eppendorf, Hamburg, Germany

²Department of Orthopedics, University Medical Center Hamburg-Eppendorf, Hamburg, Germany

³Laboratory for Anthropology and Skeletal Biology, Institute of Anatomy, Faculty of Medicine, University of Belgrade, Belgrade, Serbia

⁴Department of Trauma, Hand, and Reconstructive Surgery, University Medical Center Hamburg-Eppendorf, Hamburg, Germany

⁵Department of Forensic Medicine, University Medical Center Hamburg-Eppendorf, Hamburg, Germany

⁶Materials Sciences Division, Lawrence Berkeley National Laboratory, Berkeley, CA, USA

ABSTRACT

Immobilization as a result of long-term bed rest can lead to gradual bone loss. Because of their distribution throughout the bone matrix and remarkable interconnectivity, osteocytes represent the major mechanosensors in bone and translate mechanical into biochemical signals controlling bone remodeling. To test whether immobilization affects the characteristics of the osteocyte network in human cortical bone, femoral diaphyseal bone specimens were analyzed in immobilized female individuals and compared with age-matched postmenopausal individuals with primary osteoporosis. Premenopausal and postmenopausal healthy individuals served as control groups. Cortical porosity, osteocyte number and lacunar area, the frequency of hypermineralized lacunae, as well as cortical bone calcium content (CaMean) were assessed using bone histomorphometry and quantitative backscattered electron imaging (qBEI). Bone matrix properties were further analyzed by Fourier transform infrared spectroscopy (FTIR). In the immobilization group, cortical porosity was significantly higher, and qBEI revealed a trend toward higher matrix mineralization compared with osteoporotic individuals. Osteocyte density and canalicular density showed a declining rate from premenopausal toward healthy postmenopausal and osteoporotic individuals with peculiar reductions in the immobilization group, whereas the number of hypermineralized lacunae accumulated inversely. In conclusion, reduced osteocyte density and impaired connectivity during immobilization are associated with a specific bone loss pattern, reflecting a phenotype clearly distinguishable from postmenopausal osteoporosis. Immobilization periods may lead to a loss of survival signals for osteocytes, provoking bone loss that is even higher than in osteoporosis states, whereas osteocytic osteolysis remains absent. © 2020 The Authors. *Journal of Bone and Mineral Research* published by American Society for Bone and Mineral Research.

KEY WORDS: APOPTOSIS; BONE QUALITY; DISUSE; IMMOBILIZATION; OSTEOCYTE; UNLOADING

Introduction

Osteoporosis is the most common bone disease affecting women especially after menopause and causing increased bone fragility and fractures.⁽¹⁾ Although individuals with advanced age, female sex, and with genetic predisposition have nonmodifiable susceptibility for osteoporosis, there are modifiable risk factors that include hormone levels, nutrition, use of certain

medications, as well as lifestyle factors (smoking, alcohol consumption, physical activity).⁽¹⁾ Considering that mechanical loading is essential for bone maintenance, long-term reduced physical activity and immobilization can notably increase the risk of fracture.^(2,3) Prolonged immobilization via bed rest in hospitals and/or after an acute hospitalization is an epidemic phenomenon in elderly patients, and bed rest in this age group is associated with long-term functional impairment, muscle mass reduction,

This is an open access article under the terms of the Creative Commons Attribution License, which permits use, distribution and reproduction in any medium, provided the original work is properly cited.

Received in original form September 16, 2019; revised form December 23, 2019; accepted January 19, 2020. Accepted manuscript online January 30, 2020.

Address correspondence to: Björn Busse, PhD, Department of Osteology and Biomechanics, University Medical Center Hamburg-Eppendorf, Lottestr. 55A, 22529 Hamburg, Germany. E-mail: b.busse@uke.de

[†]TR and PM contributed equally to this work.

Journal of Bone and Mineral Research, Vol. 35, No. 7, July 2020, pp 1343–1351.

DOI: 10.1002/jbmr.3970

© 2020 The Authors. *Journal of Bone and Mineral Research* published by American Society for Bone and Mineral Research

accelerated aging, and overall negative health outcomes.⁽⁴⁾ Only 10 days of bed rest were sufficient to cause loss of 1 kg lean mass and substantial loss of lower-extremity strength in healthy aged individuals.⁽⁵⁾ Bone loss also occurs albeit at a slower rate; although insufficient data are available across age groups, it was shown in young adults that a 3-month duration of bed rest leads to decreased bone mineral density accompanied by low bone formation and increased bone resorption.⁽⁶⁾ Similarly, microgravity exposure has been found to be associated with low bone mass in humans,⁽⁷⁾ as well as decreased trabecular and cortical bone formation,^(8–10) reduced bone strength⁽¹¹⁾ and reduced bone mineralization⁽¹²⁾ in rats. However, detailed understanding of the structural basis of bedridden bone loss in aged individuals is still lacking, and it remains unknown whether the mechanisms of bone mechanical deterioration in immobilization-based osteoporosis essentially differ from postmenopausal osteoporosis in humans.

Osteocytes are the most abundant cells in bone and believed to be central regulators of bone structural and mechanical adaptation by orchestrating bone remodeling via bone-forming osteoblasts and bone-resorbing osteoclasts.⁽¹³⁾ Moreover, osteocytic osteolysis, a process where osteocytes presumably directly dissolve their surrounding matrix, receives coevally attention.⁽¹⁴⁾ The osteocytes' viability is an essential determinant of bone strength, and their apoptosis could seriously hamper bone fracture resistance.⁽¹⁵⁾ Age-dependent reduction in osteocyte number has already been demonstrated,⁽¹⁶⁾ as well as a decreased osteocyte number and osteocyte lacunar size in osteoporosis cases.^(17,18) It was shown that osteocyte apoptosis is induced by immobilization in mice,^(3,19) and there is evidence that in vitro mechanical strain by stretching or pulsatile fluid flow can prevent apoptosis in cultured osteocytes.⁽²⁰⁾ Considering the obvious importance of mechanical stimulation for osteocyte survival, immobilization with dramatic reduction in mechanical loading may lead to deteriorated bone structure in those individuals by inducing osteocyte apoptosis. Namely, it is expected that dying osteocytes would trigger osteoclastic bone resorption, whereas it is still unknown whether direct osteocytic osteolysis⁽²¹⁾ also contributes to bone loss in immobilization.⁽¹⁴⁾ Moreover, it is still unknown whether osteocyte number and lacunar interconnectivity via canaliculi are reduced in immobilized individuals that would compromise the osteocytes' mechanosensory potential and overall bone adaptation to mechanical loading conditions.⁽²²⁾ Furthermore, the presence of micropetrosis⁽²³⁾ (ie, the specific process of mineral deposition after osteocyte apoptosis leading to hypermineralized osteocyte lacuna⁽²⁴⁾ that has been identified in aged⁽¹⁶⁾ and osteoporotic bone,⁽²⁵⁾ as well as underloaded bone of auditory ossicles⁽²⁶⁾) has not been investigated in femoral cortical bone subject to immobilization and thus endangered bone quality.

Currently, the precise structural determinants of increased bone fragility in immobilization are not yet fully elucidated, and it is unknown whether immobilization-induced bone loss shares the same structural patterns with postmenopausal osteoporosis. Here we analyze the characteristics of osteocyte lacuno-canalicular network and mineralization of the femoral cortex in four groups of individuals: (i) immobilization cases, (ii) postmenopausal osteoporosis cases, (iii) postmenopausal healthy controls, and (iv) premenopausal healthy controls. We specifically focused on the cellular, structural, and compositional characteristics of human femurs, which are notably exposed to loading and unloading and are the strongest bones in the human body.^(27,28) We hypothesized that immobilization-induced bone loss is mechanistically

different from postmenopausal bone loss in osteoporosis, where immobilization leads to pronounced decay of microstructure and osteocyte characteristics.

Materials and Methods

Study cohort

Femoral bone samples were obtained from 51 female donors at autopsy within 24 hours after death. Circumstances leading to death were traumatic injuries or aging-associated diseases. Individuals suffering from cancer, renal diseases, primary hyperparathyroidism, and Paget's disease were excluded from the study. As controls, 12 healthy individuals in the young/premenopausal group (mean age 34 ± 7 years) and 9 individuals in the healthy aged/postmenopausal group (mean age 81 ± 7 years) were included. The osteoporosis group consisted of 11 women (mean age 80 ± 7 years) with manifested osteoporosis based on medical records but no documented immobilization exposure or antiresorptive osteoporosis treatment. Osteoporosis was diagnosed from the medical record and according to the World Health Organization (WHO) definition (T -score < -2.5 measured by dual-energy X-ray absorptiometry). The fourth group consisted of 19 women (mean age 83 ± 12 years) satisfying criteria of long-term immobilization, such as decubitus ulcer degree 3 or higher, muscle contractures, and documented long-term bed rest in their medical record for more than 3 months, respectively. These immobilization criteria were checked precisely during autopsy and from medical records. Approval to obtain the specimens for this study was obtained. The study was approved by the local ethics committee (Hamburg Chamber of Physicians) under WF-05/16.

Bone sample preparation

The femoral bone specimens were cut in cross sections 11 cm inferior to the greater trochanter and the lateral quadrant of the section was further processed for all the analyses (Fig. 1A–F). At this point, the entire bone is cortical. These cross sections were fixed in 3.7% formaldehyde for 3 days, dehydrated with an ascending alcohol series, and embedded in methyl-methacrylate. Embedded specimens were cut on a Microtec rotation microtome (Techno-Med GmbH, Munich, Germany) in sections of $5 \mu\text{m}$ and were subsequently stained with toluidine blue.

Histological analysis

Osteocyte measurements were performed using a Zeiss bright-field microscope (Carl Zeiss Vision GmbH, Jena, Germany) equipped with an Osteomeasure system (Osteometrics, Atlanta, GA, USA). All cellular and structural indices were measured according to the ASBMR nomenclature committee.⁽²⁹⁾ Ten visual fields were sampled per defined bone area ($20\times$ objective) by moving the specimen in equally sized steps in the x and y directions. In this way, a total bone area of approximately 1 mm^2 per subject was measured to determine lacunar and osteocyte numbers. The number of lacunae occupied by osteocytes and the number of empty lacunae per bone area were measured in the cortical bone. Viable osteocytes appeared as cells with dark blue stained cell nucleus, whereas empty lacunae were defined as lacunae without any visible cell remnants. The parameters were quantified as described previously⁽³⁰⁾ the number of lacunae occupied by osteocyte cell nucleus per bone area (N.Ot/B.Ar, $1/\text{mm}^2$), number of empty lacunae per bone area (N.Empt.Lc/B.Ar, $1/\text{mm}^2$), fraction of empty lacunae (number of

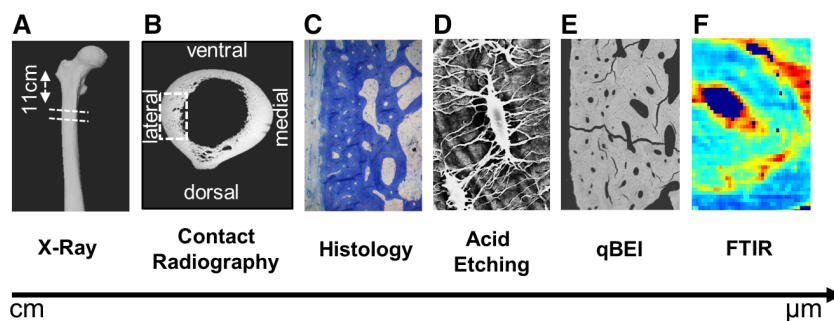


Fig. 1. Multiscale assessment of cortical bone properties. (A) Cross sections were obtained 11 cm inferior to the greater trochanter (overview shown with X-ray imaging). (B) Contact radiography of the cross sections and marking of the lateral quadrant where analyses were performed. (C, D) Assessment of osteocytes and lacunar canaliculi via histology and acid etching. (E, F) Matrix composition determined via quantitative backscattered electron imaging (qBEI) and Fourier transform infrared spectroscopy (FTIR).

empty lacunae/total number of lacunae, %), and total lacunar number per bone area (Tt.Lc.N/B.Ar, $1/\text{mm}^2$).

Quantitative backscattered electron imaging (qBEI)

After preparing histological sections, the embedded bone samples from the lateral quadrant of the cross section were polished to a coplanar finish and carbon coated. Quantitative backscattered electron imaging was performed, as described previously,^(16,31,32) using a scanning electron microscope (LEO 435 VP; LEO Electron Microscopy Ltd., Cambridge, UK) with a backscattered electron detector (Type 202; K.E. Developments Ltd., Cambridge, UK). The scanning electron microscope was operated at 20 kV and 665 pA at a constant working distance. Three images per specimen were acquired and further analyzed using ImageJ analysis software (ImageJ 1.42, National Institutes of Health, Bethesda, MD, USA). The total analyzed area was 5 mm^2 per specimen. As the generated gray values represent the mean calcium content (mean Ca-Wt%) of the cross-sectioned bone,⁽³¹⁾ the technique was used to measure the bone mineral density distribution but also to image and analyze the osteocyte lacunae. For each sample, the cortical porosity (Ct.Po), the mean calcium content (CaMean), peak calcium content (CaPeak), mineralization heterogeneity (CaWidth), the number of osteocyte lacunae per bone area (Tt.Lc.N/B.Ar), and mean osteocyte lacunar area (Lc.Ar) were measured using a custom MATLAB-based program (TheMathWorks, Inc., Natick, MA, USA), while the number of hypermineralized osteocyte lacunae per bone area (N.Mn.Lc/B.Ar) were quantified in ImageJ.

Acid etching

Acid etching of the embedded human cortical bone was performed, as reported previously^(22,30) and following the report of Kubek and colleagues.⁽³³⁾ Briefly, the specimens were immersed in 9% phosphoric acid, deionized water, and eventually exposed to 5% sodium hypochlorite. Subsequently they were dried, sputter coated with gold, and imaged by scanning electron microscopy. The number of canalicular profiles per osteocyte lacuna (N.Ot.Ca profiles/Lc) and the mean value of maximum canalicular lengths (Ca.Le) were measured from the obtained images using ImageJ. Maximum canalicular length corresponds to the length of the longest visible canaliculi in each of the analyzed osteons

with the criteria that measured canaliculi reach the outermost lamella of the specific osteon.

Fourier transform infrared spectroscopy (FTIR)

For further bone compositional analysis, mineral and matrix characterization via FTIR was performed. Each specimen was scanned at the periosteal region using attenuated total reflectance (ATR) mode of a Frontier FTIR spectrometer (Universal ATR, Perkin Elmer, Waltham, MA, USA). Spectra were acquired over a spectral range of 4000 to 570 cm^{-1} . Each spectrum was acquired 12 times, automatically averaged for better signal to noise ratio and background subtracted using the software of the manufacturer (Spectrum v. 10.4.4.449, PerkinElmer). Images were acquired using the ATR mode of a Spotlight 400 (PerkinElmer) attached to the Frontier FTIR spectrometer with 8 scans per pixel at the same spectral range of 4000 to 570 cm^{-1} . Further data processing was carried out using a customized MATLAB routine. Automatic PMMA correction^(34,35) was performed at the region of 1790 cm^{-1} for weighting the contribution of PMMA to the measured spectrum and subtracting it. Mineral-to-matrix ratio was calculated by dividing the area of the phosphate peak ($1154\text{--}900 \text{ cm}^{-1}$) by the area of the amide I peak ($1710\text{--}1600 \text{ cm}^{-1}$).^(35–37) Carbonate-to-phosphate ratio was determined by dividing the area of the peak at $890\text{--}850 \text{ cm}^{-1}$ and $1154\text{--}900 \text{ cm}^{-1}$.^(35–37) Matrix maturity ratio was calculated after subpeak fitting the amide I peak with respect to the second derivative and dividing the subpeak areas at 1661 cm^{-1} and 1692 cm^{-1} .⁽³⁵⁾

Statistical analysis

SPSS version 15 (SPSS, Inc., Chicago, IL, USA) was used for statistical analysis. The Kolmogorov–Smirnov test was applied to test for normal distribution. One-way analysis of variance (ANOVA) was performed to check for significant differences in the evaluated parameters between four groups (young, aged, osteoporosis, and immobilization). If the ANOVA results were significant, post hoc tests were carried out using a Bonferroni correction for multiple comparisons. To specifically analyze differences in the morphological pattern of osteoporosis and immobilization groups, for each analyzed parameter the pooled values of both groups were binarized (classified by the numerical values to those below versus those equal or higher than the common mean value of both groups pooled). Chi-square test (or Fisher's

exact probability test if there was at least one cell with expected frequency below 5) was then used to evaluate whether osteoporosis and immobilization groups showed different distribution of values in relation to the common mean. In all the analyses, a p value of 0.05 or less was considered as statistically significant.

Results

High cortical porosity along with low number of osteocytes and high fraction of empty lacunae in immobilization cases

The cortical porosity in the femoral diaphysis showed a linear trend ($p < .001$) from the lowest values in the young group ($5.0 \pm 1.9\%$) to very high porosity values in the immobilization group ($20.0 \pm 7.3\%$). The immobilization group showed significantly higher values than osteoporosis, aged, and young cases ($p = .035, p < .001, p < .001$, respectively) (Fig. 2A, B). Histological measurements of the osteocyte number per bone area revealed a significant declining trend from the premenopausal ($205.2 \pm 41.4/\text{mm}^2$) to the immobilization group ($92.3 \pm 16.5/\text{mm}^2$) ($p < .001$), whereas the fraction of empty lacunae per total lacunae showed the opposite trend ($p < .001$) with $32.0 \pm 7.2\%$ of empty lacunae in the premenopausal group versus $53.2 \pm 6.4\%$ in immobilization group (Fig. 2C–F). Moreover, we were able to detect a significantly lower number of total

osteocyte lacunae in the immobilization cases than in the young, aged, and osteoporosis groups, as determined in histological sections ($p < .001, p = .008, p = .053$, respectively). Chi-square or Fisher's test revealed that the immobilization group was mostly distributed in the top 50th percentile (above median) in terms of cortical porosity values ($p = .058$) and fraction of empty lacunae ($p = .021$), whereas osteocyte density values ($p = .05$) and osteocyte lacunar density values ($p = .005$) were located in the lower 50th percentile (below median), when compared with the osteoporosis group.

Lower mineralization heterogeneity in immobilization compared with osteoporosis

The overall bone mineral density distribution (BMDD) assessed by backscattered signal intensities was only marginally altered between young and immobilized bone, yet tended to differ from the osteoporotic BMDD (Fig. 3A). The mean calcium content (CaMean) was lowest in the osteoporosis group (24.71 ± 0.65 wt %), but without reaching statistical significance between the groups ($p = .197$). CaMean and CaPeak in the immobilization group were similar to the young and old cases (Fig. 3C, D). Mineralization heterogeneity in terms of CaWidth differed significantly between the groups ($p = .008$), tending to lower values in the immobilization than in osteoporosis cases ($p = .079$), indicating an overall low bone remodeling state during immobilization

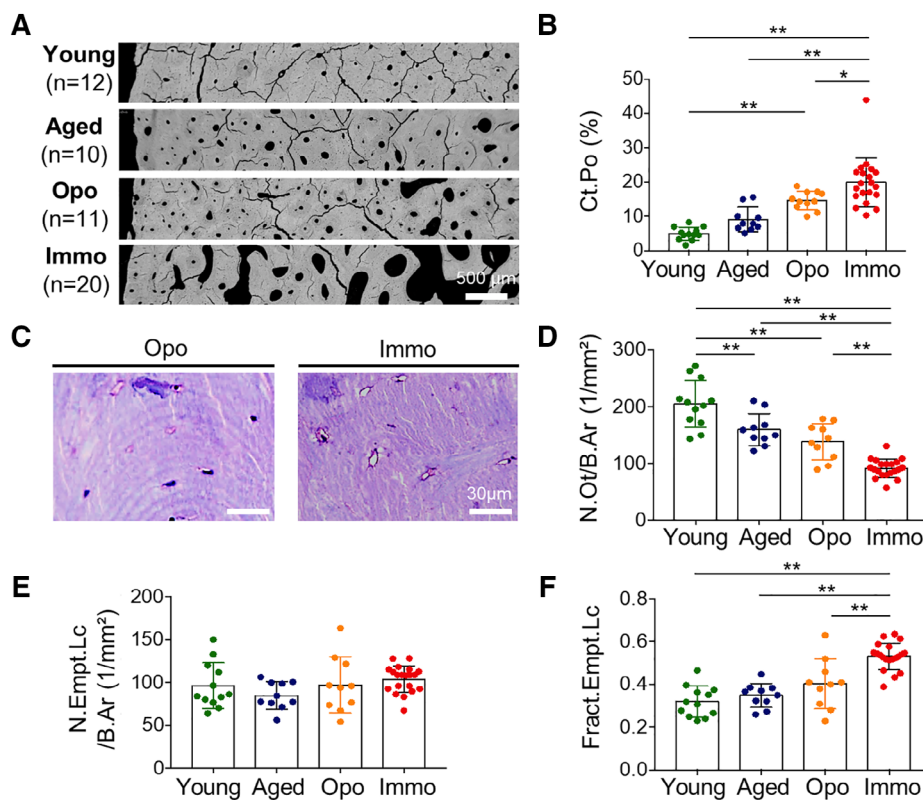


Fig. 2. Cortical porosity and osteocyte characteristics. (A) Degree of cortical porosity between young, aged, osteoporotic (Opo), and immobilized (Immo) individuals shown in qBEI images. (B) Substantially increased cortical porosity with immobilization. (C) Histological images of toluidine blue-stained bone sections illustrating reduced number of osteocyte lacunae and predominance of empty lacunae in immobilization compared with the osteoporosis group. (D) Lower number of osteocytes per bone area with immobilization. (E) No significant differences in number of empty lacunae per bone area, but a higher fraction of empty lacunae with immobilization is evident (F). * $p < .05$, ** $p < .01$.

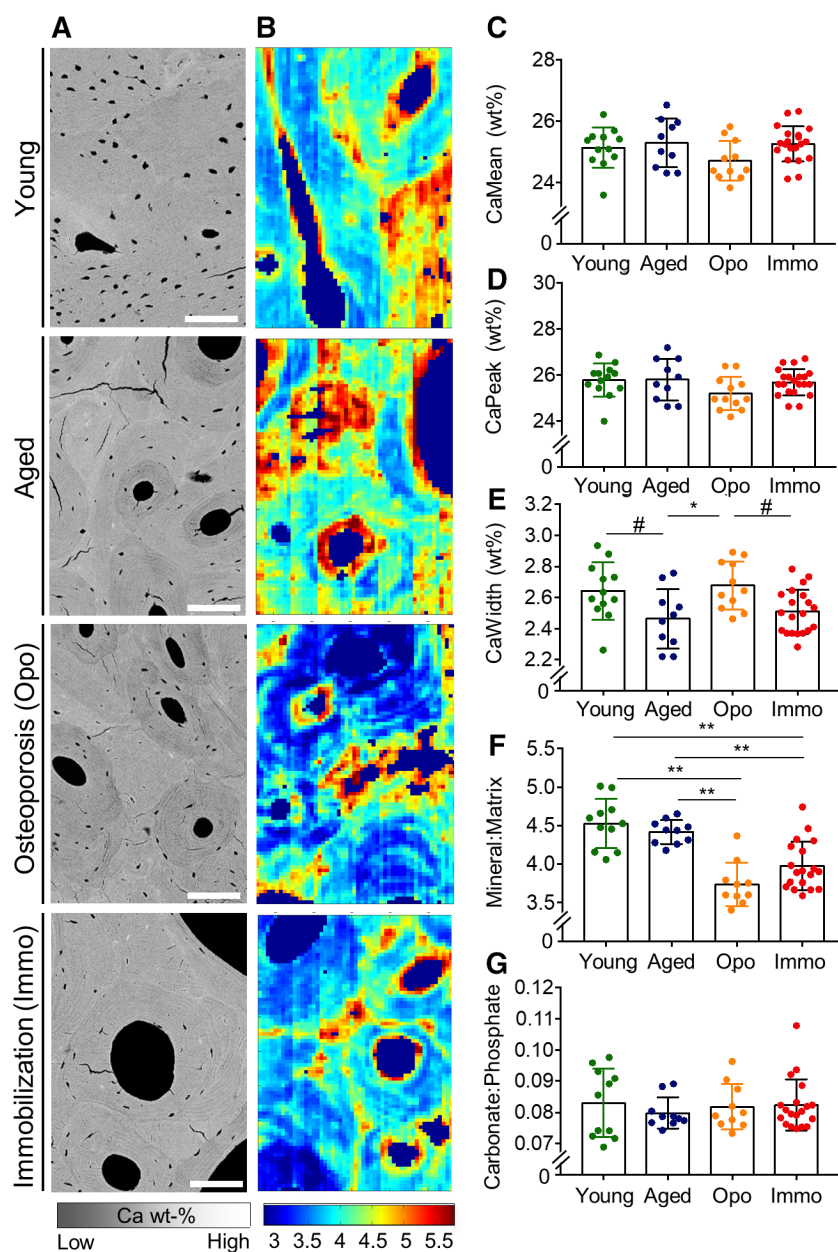


Fig. 3. Bone mineral density distribution and bone matrix composition. (A) BMDD values were calculated from the backscattered signal intensities as shown in the exemplary images. (B) Representative FTIR maps reflecting the mineral-to-matrix ratio in the four study groups. (C) Degree of mineralization reflected by calcium mean values. (D) Calcium peak values between the different groups. (E) Mineralization heterogeneity in terms of CaWidth shows increased mineral heterogeneity in postmenopausal osteoporosis than in immobilization. (F) The mineral-to-matrix ratio was significantly lower in postmenopausal osteoporosis and immobilization compared with young cases, although a tendency toward higher mineralization was noted in immobilization. (G) Carbonate-to-phosphate ratio. * $p < .05$, ** $p < .01$, # $.05 < p < .1$.

(Fig. 3E). Chi-square/Fisher's test revealed that the immobilization group tended to be mostly distributed within the top 50th percentile of CaMean and CaPeak values ($p = .058$, $p = .063$), whereas the CaWidth ($p = .058$) values were found in the lower 50th percentile, when compared with the osteoporosis group.

The ratio of bone mineral per collagenous matrix was measured using the FTIR-based mineral-to-matrix ratio (Fig. 3B). Here osteoporotic bone revealed the lowest mineral-to-matrix ratio (3.74 ± 0.28) adding additional information to the qBEI data pointing toward a lower mineral content, whereas the highest

mineral-to-matrix ratio (4.53 ± 0.32) (Fig. 3F) was found in the group of young individuals. The mineral-to-matrix ratio in immobilization and osteoporosis groups was lower than in young and aged groups ($p < .05$ each). The carbonate-to-phosphate ratio did not differ between the groups, indicating an equal mineral maturity at the measured region ($p = .864$, Fig. 3G). Additionally, to quantify the collagen quality, the matrix maturity was evaluated but did not show any significant differences among the groups ($p = .952$). Based on the Chi-square test, there was a tendency showing that the immobilization group's mineral-to-matrix ratios

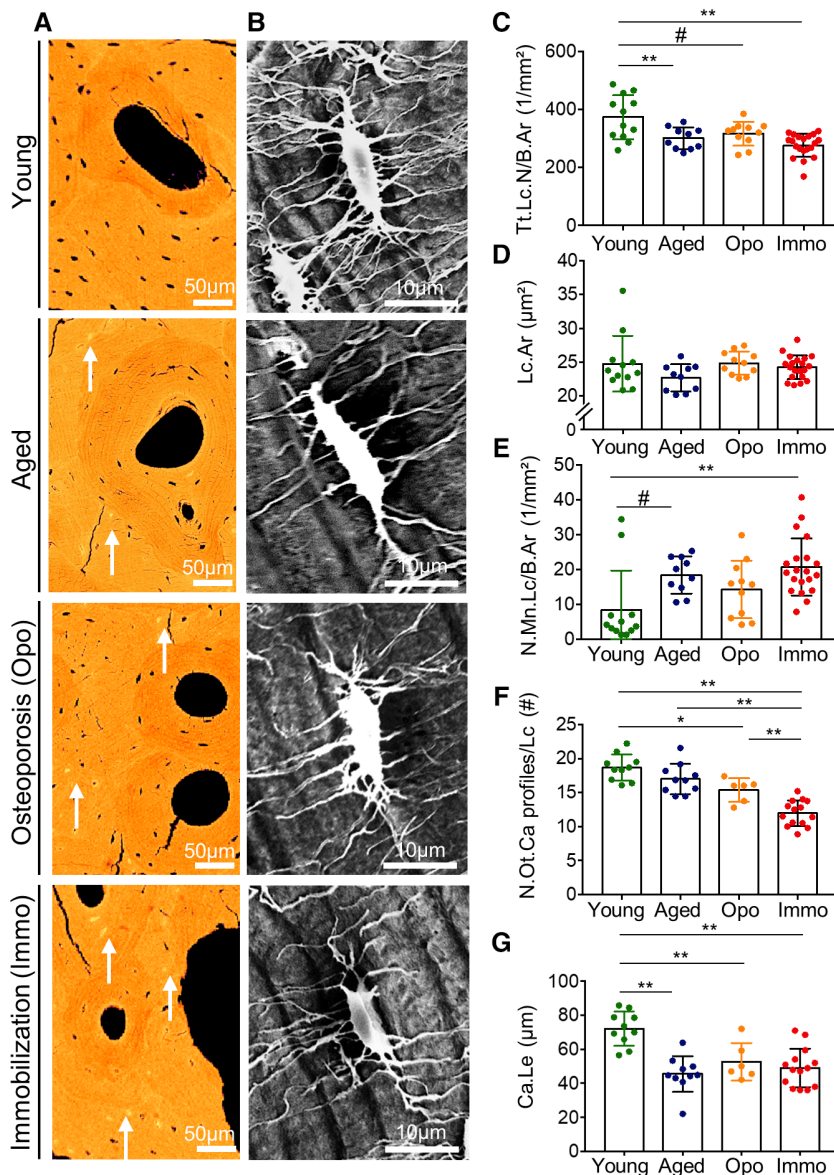


Fig. 4. Osteocyte lacunar and canalicular characteristics. (A) Reduction of osteocyte number and size as well as the increase of micropetrotic lacunae (white arrows) are evident in qBEI images from young to immobilization group. (B) Osteocyte lacunae were imaged using acid-etching and subsequent SEM to quantify the osteocyte canalicular profiles. (C) The total lacunar number decreased significantly between young and immobilized cases. (D) Lacunar area was not different between the groups. (E) The number of mineralized lacunae is the lowest in the young group and then show rising numbers with reaching a maximum in immobilization. (F) The number of osteocyte canalicular profiles per lacuna is high in the young group and then shows a declining rate. The lowest number of canalicular profiles was found in the immobilization cases. (G) Canalicular mean maximum length measured between outermost lacuna to the Haversian canal is highest in the young group. * $p < .05$, ** $p < .01$, # $.05 < p < .1$.

were distributed in the top 50th percentile in comparison to the distribution of the mineral-to-matrix ratios of the osteoporosis group ($p = .115$).

Low canalicular number and high density of micropetrotic lacunae in immobilization

A decline of total osteocyte lacunar density in aged, osteoporosis, and immobilization groups compared with the young ($p = .007$, $p = .059$, $p < .001$, respectively) group was confirmed by back-scattered electron microscopy (Fig. 4A, C). The lacunar area

(Lc.Ar) did not show significant intergroup differences ($p = .327$; Fig. 4D). Highly mineralized (micropetrotic) osteocyte lacunae were most frequently found in immobilized cases ($20.7 \pm 8.5/\text{mm}^2$), significantly higher than in the young group ($8.4 \pm 11.2/\text{mm}^2$) ($p = .002$) (Fig. 4E).

The analysis of canalicular connections by acid etching and subsequent scanning electron microscopy of the plastic-embedded bone revealed that the number of osteocyte canalicular profiles per osteocyte lacuna was lower in the immobilization group than in the young, aged, and osteoporosis group ($p < .001$, $p < .001$, $p = .008$) (Fig. 4F). Canalicular mean maximum

length was higher in the young group than in the other three study groups ($p < .05$) (Fig. 4G).

Chi-square/Fisher's test revealed that in contrast to the osteoporosis group, the immobilization group tended to be distributed within the lower 50th percentile of values for Ot.Lc.N/B.Ar ($p = .058$) and N.Ot.Ca profiles/Lc ($p = .141$), as well as in the top 50th percentile of the values for Mn.Lc.N/B.Ar ($p = .058$).

Discussion

The present study on healthy and diseased human cortical bone was carried out to assess the effects of immobilization on osteocyte density and characteristics compared with postmenopausal osteoporosis as well as to young and aged individuals and to healthy reference subjects. Next to the increased cortical porosity and higher matrix mineralization, immobilization cases showed a lower osteocyte density accompanied by a higher proportion of empty lacunae, which reflects an increased osteocyte death in immobilization when compared with postmenopausal osteoporosis. Increased osteocyte death was also reflected in exceptionally high numbers of mineralized lacunae per bone area found in immobilization cases. Our *ex situ* findings in immobilization patients are in agreement with the data from *in vitro* studies having reported that mechanical forces provide signals to maintain osteocyte viability, so that lack of mechanical stimulation is followed by apoptosis.^(19,20,38) Dying osteocytes, conversely, presumably trigger osteoclast recruitment, thus resulting in increased bone resorption and bone loss as reflected in increasing cortical porosity in our study. As a consequence of a reduced osteocyte lacuno-canalicular network that we showed in this study (ie, lower number of osteocyte lacunae, fewer viable osteocytes, fewer canalicular connections), there is substantial risk for impaired mechanosensitivity⁽²²⁾ and decreased detection of microcracks.⁽³⁹⁾ Moreover, the remarkable high number of hypermineralized osteocyte lacunae underline the failure of bone remodeling in immobilized human bone, as it was previously shown in conditions with specific skeletal loading scenarios: periosteal and endocortical cortices of aged bone,⁽¹⁶⁾ osteoarthritic bone,⁽⁴⁰⁾ as well as in the human auditory ossicles that are subject to limited mechanical loading.⁽²⁶⁾ The high percentages of empty osteocyte lacunae measured in osteoporosis and immobilization group was comparable to the data reported by Power and colleagues in the femoral neck of elderly individuals with and without a fracture.⁽⁴¹⁾

A major messenger involved in these reorganization processes is the anti-anabolic protein sclerostin,⁽⁴²⁾ which inhibits bone formation and which was reported to be elevated during bed rest as well as by mechanical unloading in osteocytes *in vitro*.^(43,44) Locally elevated levels of sclerostin may explain the higher mineralization in immobilized cases, since the dissociation of high bone resorption and low bone formation is accompanied by insufficient replacement of bone and subsequent aging of the bone tissue. This would also have therapeutic consequences, as one would favor sclerostin antibodies⁽⁴⁵⁾ in immobilization-induced osteoporosis. The osteocyte death by immobilization could not only be an effect of unloading itself but also of the apparent muscle atrophy in immobilization as muscle and bone are subjects of an effective molecular cross-talk.^(46,47)

The analysis of bone mineral density distribution and FTIR spectroscopy in the femoral cortex showed that immobilized bone exhibited slightly higher bone mineralization than osteoporotic bone. Generally, while higher tissue age is associated

with a higher degree of mineralization,^(48–50) aged and osteoporotic individuals usually show lower calcium content due to a high remodeling rate, thus replacing old tissue by newly built bone tissue at a lower mineralization.⁽²⁵⁾ Our results confirmed lower mean calcium content in the cohort of postmenopausal osteoporosis, whereas in the immobilization group, the mineral content was found to be in the range of young control specimens. However, CaWidth as a measure of matrix mineralization heterogeneity tended to be lower in the immobilization cases than in the osteoporosis cases, indicating that the high matrix mineralization in immobilization is due to absence of newly formed bone at bone surfaces. However, FTIR imaging revealed that although the mineral content in immobilized bone was higher than in osteoporosis cases, interestingly there was no increase in degree of carbonate substitution in hydroxyapatite (evident through the unchanged carbonate-to-phosphate ratio) and no change in the matrix and collagen quality. Obviously, the bone exposed to immobilization featured a different mineralization pattern than osteoporotic bone, which underlines that the mechanism of bone loss might be different.

Our results are in contrast to the observation that increased osteocyte perilacunar remodeling is one major process contributing to bone loss in immobilization.⁽⁵¹⁾ In fact, the osteocyte lacunar size in immobilized individuals did not differ from the controls and osteoporosis. Because immobilization may lead to hypercalcemia⁽⁶⁾ due to osteoclastic resorption, we propose that in this condition lacunar remodeling is suppressed to a minimum level since there is no need for additional calcium removal around the osteocyte lacunae as opposed to, for example, lactation⁽⁵²⁾ or vitamin D deficiency,^(30,53) both conditions in which osteocyte lacunar areas are increased. Our findings of unchanged lacunar area are compatible with experiments in rats.⁽⁵⁴⁾ Namely, Bach-Gansmo and colleagues⁽⁵⁴⁾ reported that the bone architecture and not osteocyte lacunar properties dominated the bones' response to immobilization as well as the subsequent recovery in rats. However, although osteocyte lacunar area was unchanged, we found further peculiar impairment of osteocyte characteristics as a hallmark of immobilization in humans, which was not found in animal studies. In particular, mineralization of osteocyte lacunae occurs exclusively in human bone and not in rodent bone.⁽¹⁶⁾ Osteocyte characteristics derived from experiments in rodents should be taken with caution because they do not reflect the width of changes in terms of osteocyte lacunar properties in humans.

The observed changes in bone material composition indicate impaired mechanosensitive behavior of immobilized bone. In addition, considering that ANOVA intergroup differences were more visible in mineral-to-matrix ratio than in CaMean, it seems that mineral-to-matrix ratio is a highly sensitive parameter when detecting compositional and mechanical alterations in conditions of aging, osteoporosis, and immobilization. The influence of immobilization on the mechanical properties of bone pinpoints the need of musculoskeletal loading during states of immobilization.^(55,56)

The study has a few limitations: Clinical fracture risk assessment by osteodensitometry could not be performed in the immobilization group (autopsy cases). Nevertheless, the histological analysis of the immobilization group showed a striking increase in cortical porosity compared with both the controls and the postmenopausal osteoporosis group. Furthermore, we did not measure biochemical or histomorphometric markers of bone turnover (eg, CTX, DPD, number of osteoblasts/osteoclasts) or calcium homeostasis because this was a postmortem study

focusing on the micromorphology and osteocyte characteristics. In this study, we have focused predominantly on one anatomical quadrant of a femoral cross section. As other quadrants may show specific morphological patterns due to different loading conditions, future studies should include regions of interest in relation to habitual loading. The absolute canalicular numbers per lacuna in our assessment by SEM on acid-etched plastic-embedded specimens are certainly lower than in a full 3D assessment using synchrotron nanoCT⁽⁵⁷⁾ or FIB-SEM.⁽⁵⁸⁾ However, preparing and analyzing all specimens in a consistent manner ensured reliable intergroup comparisons. One advantage of the SEM approach applied here compared with SR-nanoCT or FIB-SEM is that a higher number of cases and larger bone areas could be assessed per time period, while the visualization of almost all canalliculi per lacunae provides valuable 3D information.⁽⁵⁷⁾

In conclusion, although the morphological patterns of postmenopausal osteoporosis and immobilization share some characteristics, we identified that there is a mechanistically distinct pathology indicating that individuals subject to immobilization show significantly higher cortical porosity with tremendous osteocyte death and lacunar mineralization (ie, micropetrosis), while there is no evidence of osteocytic osteolysis in a highly mineralized matrix of immobilized bone.

Disclosures

All authors state that they have no conflicts of interest.

Acknowledgments

FS acknowledges a PhD fellowship of the Joachim Herz Stiftung in cooperation with PIER (Partnership in Innovation, Education and Research) a program of the University of Hamburg and DESY. The authors thank Christoph Riedel for support on the Matlab programming for qBEI. PM and BB acknowledge the institutional partnership support from the Alexander von Humboldt Foundation. TR is supported by the German Research Foundation under grant no. RO 5925/1-1. PM is supported by the Serbian Ministry of Education and Science (III45005). BB is supported by the German Research Foundation (DFG) under grant no. BU 2562/3-1/5-1.

Authors' roles: Study design: TR, MA, and BB. Autopsy and specimen collection: BW, EMW, and KP. Data collection: TR, MK, and FNS. Data analysis: TR, PM, FNS, SVK, and BB. Data interpretation: TR, PM, FNS, SVK, EMW, ROR, MA, and BB. Drafting manuscript: TR, PM, and BB. Approving final version of manuscript: TR, PM, FNS, SVK, EMW, MK, BW, KP, ROR, MA, and BB. TR takes responsibility for the integrity of the data analysis.

References

- Rachner TD, Khosla S, Hofbauer LC. Osteoporosis: now and the future. *Lancet*. 2011;377(9773):1276–87.
- Bikle DD, Sakata T, Halloran BP. The impact of skeletal unloading on bone formation. *Gravit Space Biol Bull*. 2003;16(2):45–54.
- Tatsumi S, Ishii K, Amizuka N, et al. Targeted ablation of osteocytes induces osteoporosis with defective mechanotransduction. *Cell Metab*. 2007;5(6):464–75.
- Kehler DS, Theou O, Rockwood K. Bed rest and accelerated aging in relation to the musculoskeletal and cardiovascular systems and frailty biomarkers: a review. *Exp Gerontol*. 2019;124:110643.

- Kortebein P, Symons TB, Ferrando A, et al. Functional impact of 10 days of bed rest in healthy older adults. *J Gerontol, Ser A*. 2008; 63(10):1076–81.
- Zerwekh JE, Ruml LA, Gottschalk F, Pak CY. The effects of twelve weeks of bed rest on bone histology, biochemical markers of bone turnover, and calcium homeostasis in eleven normal subjects. *J Bone Miner Res*. 1998;13(10):1594–601.
- Vico L, Collet P, Guignandon A, et al. Effects of long-term microgravity exposure on cancellous and cortical weight-bearing bones of cosmonauts. *Lancet*. 2000;355(9215):1607–11.
- Wronski TJ, Morey ER. Effect of spaceflight on periosteal bone formation in rats. *Am J Physiol*. 1983;244(3):R305–9.
- Turner RT, Evans GL, Wakley GK. Spaceflight results in depressed cancellous bone formation in rat humeri. *Aviat Space Environ Med*. 1995; 66(8):770–4.
- Pajevic PD, Spatz JM, Garr J, Adamson C, Misener L. Osteocyte biology and space flight. *Curr Biotechnol*. 2013;2(3):179–83.
- Spengler DM, Morey ER, Carter DR, Turner RT, Baylink DJ. Effects of spaceflight on structural and material strength of growing bone. *Proc Soc Exp Biol Med*. 1983;174(2):224–8.
- Turner RT, Bell NH, Duvall P, et al. Spaceflight results in formation of defective bone. *Proc Soc Exp Biol Med*. 1985;180(3):544–9.
- Bonewald LF. Osteocytes as dynamic multifunctional cells. *Ann N Y Acad Sci*. 2007;1116:281–90.
- Tsourdi E, Jahn K, Rauner M, Busse B, Bonewald LF. Physiological and pathological osteocytic osteolysis. *J Musculoskelet Neuronal Interact*. 2018;18(3):292–303.
- Milovanovic P, Busse B. Inter-site variability of the human osteocyte lacunar network: implications for bone quality. *Curr Osteoporosis Rep*. 2019;17(3):105–15.
- Busse B, Djonic D, Milovanovic P, et al. Decrease in the osteocyte lacunar density accompanied by hypermineralized lacunar occlusion reveals failure and delay of remodeling in aged human bone. *Aging Cell*. 2010;9(6):1065–75.
- Mullender MG, van der Meer DD, Huiskes R, Lips P. Osteocyte density changes in aging and osteoporosis. *Bone*. 1996;18(2):109–13.
- Qiu S, Rao DS, Palnitkar S, Parfitt AM. Reduced iliac cancellous osteocyte density in patients with osteoporotic vertebral fracture. *J Bone Miner Res*. 2003;18(9):1657–63.
- Aguirre JI, Plotkin LI, Stewart SA, et al. Osteocyte apoptosis is induced by weightlessness in mice and precedes osteoclast recruitment and bone loss. *J Bone Miner Res*. 2006;21(4):605–15.
- Bakker A, Klein-Nulend J, Burger E. Shear stress inhibits while disuse promotes osteocyte apoptosis. *Biochem Biophys Res Commun*. 2004;320(4):1163–8.
- Teti A, Zallone A. Do osteocytes contribute to bone mineral homeostasis? Osteocytic osteolysis revisited. *Bone*. 2009;44(1):11–6.
- Milovanovic P, Zimmermann EA, Hahn M, et al. Osteocytic canalicular networks: morphological implications for altered mechanosensitivity. *ACS Nano*. 2013;7(9):7542–51.
- Frost H. Micropetrosis. *J Bone Joint Surg Am*. 1960;42:144–50.
- Milovanovic P, Zimmermann EA, Vom Scheidt A, et al. The formation of calcified nanospherites during micropetrosis represents a unique mineralization mechanism in aged human bone. *Small*. 2017;13(3): 1602215.
- Milovanovic P, Zimmermann EA, Riedel C, et al. Multi-level characterization of human femoral cortices and their underlying osteocyte network reveal trends in quality of young, aged, osteoporotic and antiresorptive-treated bone. *Biomaterials*. 2015;45:46–55.
- Rolvien T, Schmidt FN, Milovanovic P, et al. Early bone tissue aging in human auditory ossicles is accompanied by excessive hypermineralization, osteocyte death and micropetrosis. *Sci Rep*. 2018;8(1):1920.
- Ettinger B, Burr DB, Ritchie RO. Proposed pathogenesis for atypical femoral fractures: lessons from materials research. *Bone*. 2013;55(2): 495–500.
- Busse B, Hahn M, Schinke T, Püschel K, Duda GN, Amling M. Reorganization of the femoral cortex due to age-, sex-, and endoprosthetic-related effects emphasized by osteonal dimensions and remodeling. *J Biomed Mater Res A*. 2010;92(4):1440–51.

29. Dempster DW, Compston JE, Drezner MK, et al. Standardized nomenclature, symbols, and units for bone histomorphometry: a 2012 update of the report of the ASBMR Histomorphometry Nomenclature Committee. *J Bone Miner Res.* 2013;28(1):2–17.
30. Rolvien T, Krause M, Jeschke A, et al. Vitamin D regulates osteocyte survival and perilacunar remodeling in human and murine bone. *Bone.* 2017;103:78–87.
31. Roschger P, Paschalis EP, Fratzl P, Klaushofer K. Bone mineralization density distribution in health and disease. *Bone.* 2008;42(3):456–66.
32. Zimmermann EA, Riedel C, Schmidt FN, et al. Mechanical competence and bone quality develop during skeletal growth. *J Bone Miner Res.* 2019;34(8):1461–72.
33. Kubek DJ, Gattone VH 2nd, Allen MR. Methodological assessment of acid-etching for visualizing the osteocyte lacunar-canalicular networks using scanning electron microscopy. *Microsc Res Tech.* 2010;73(3):182–6.
34. Pleshko NL, Boskey AL, Mendelsohn R, An FT-IR. Microscopic investigation of the effects of tissue preservation on bone. *Calcif Tissue Int.* 1992;51(1):72–7.
35. Schmidt FN, Zimmermann EA, Campbell GM, et al. Assessment of collagen quality associated with non-enzymatic cross-links in human bone using Fourier-transform infrared imaging. *Bone.* 2017;97:243–51.
36. Boskey A, Pleshko CN. FT-IR imaging of native and tissue-engineered bone and cartilage. *Biomaterials.* 2007;28(15):2465–78.
37. Schmidt FN, Delsmann MM, Mletzko K, et al. Ultra-high matrix mineralization of sperm whale auditory ossicles facilitates high sound pressure and high-frequency underwater hearing. *Proc R Soc Lond B Biol Sci.* 2018;285(1893):20181820.
38. Noble BS, Peet N, Stevens HY, et al. Mechanical loading: biphasic osteocyte survival and targeting of osteoclasts for bone destruction in rat cortical bone. *Am J Physiol Cell Physiol.* 2003;284(4):C934–43.
39. Qiu S, Rao DS, Fyhrie DP, Palnitkar S, Parfitt AM. The morphological association between microcracks and osteocyte lacunae in human cortical bone. *Bone.* 2005;37(1):10–5.
40. Carpentier VT, Wong J, Yeap Y, et al. Increased proportion of hypermineralized osteocyte lacunae in osteoporotic and osteoarthritic human trabecular bone: implications for bone remodeling. *Bone.* 2012;50(3):688–94.
41. Power J, Noble BS, Loveridge N, Bell KL, Rushton N, Reeve J. Osteocyte lacunar occupancy in the femoral neck cortex: an association with cortical remodeling in hip fracture cases and controls. *Calcif Tissue Int.* 2001;69(1):13–9.
42. Li X, Zhang Y, Kang H, et al. Sclerostin binds to LRP5/6 and antagonizes canonical Wnt signaling. *J Biol Chem.* 2005;280(20):19883–7.
43. Spatz JM, Fields EE, Yu EW, et al. Serum sclerostin increases in healthy adult men during bed rest. *J Clin Endocrinol Metab.* 2012;97(9):E1736–40.
44. Spatz JM, Wein MN, Gooi JH, et al. The Wnt inhibitor Sclerostin is up-regulated by mechanical unloading in osteocytes in vitro. *J Biol Chem.* 2015;290(27):16744–58.
45. McClung MR, Grauer A, Boonen S, et al. Romosozumab in postmenopausal women with low bone mineral density. *N Engl J Med.* 2014;370(5):412–20.
46. Jahn K, Lara-Castillo N, Brotto L, et al. Skeletal muscle secreted factors prevent glucocorticoid-induced osteocyte apoptosis through activation of beta-catenin. *Eur Cells Mater.* 2012;24:197–209 discussion–10.
47. Bonewald LF. Does defective bone lead to defective muscle? *J Bone Miner Res.* 2015;30(4):593–5.
48. Koehne T, Vettorazzi E, Kusters N, et al. Trends in trabecular architecture and bone mineral density distribution in 152 individuals aged 30–90 years. *Bone.* 2014;66:31–8.
49. Milovanovic P, vom Scheidt A, Mletzko K, et al. Bone tissue aging affects mineralization of cement lines. *Bone.* 2018;110:187–93.
50. Schmidt FN, Zimmermann EA, Walsh F, et al. On the origins of fracture toughness in advanced teleosts: how the Swordfish Sword's bone structure and composition allow for slashing under water to kill or Stun Prey. *Adv Sci.* 2019;6(12):1900287.
51. Blaber EA, Dvorochkin N, Lee C, et al. Microgravity induces pelvic bone loss through osteoclastic activity, osteocytic osteolysis, and osteoblastic cell cycle inhibition by CDKN1a/p21. *PLoS One.* 2013;8(4):e61372.
52. Jähn K, Kelkar S, Zhao H, et al. Osteocytes acidify their microenvironment in response to PTHrP in vitro and in lactating mice in vivo. *J Bone Miner Res.* 2017;32(8):1761–72.
53. Busse B, Bale HA, Zimmermann EA, et al. Vitamin D deficiency induces early signs of aging in human bone, increasing the risk of fracture. *Sci Transl Med.* 2013;5(193):193ra88.
54. Bach-Gansmo FL, Wittig NK, Bruel A, Thomsen JS, Birkedal H. Immobilization and long-term recovery results in large changes in bone structure and strength but no corresponding alterations of osteocyte lacunar properties. *Bone.* 2016;91:139–47.
55. Fiedler IAK, Schmidt FN, Wölfel EM, et al. Severely impaired bone material quality in chihuahua zebrafish resembles classical dominant human osteogenesis imperfecta. *J Bone Miner Res.* 2018;33(8):1489–99.
56. Picke A-K, Sylow L, Møller LLV, et al. Differential effects of high-fat diet and exercise training on bone and energy metabolism. *Bone.* 2018;116:120–34.
57. Varga P, Hesse B, Langer M, et al. Synchrotron X-ray phase nanotomography-based analysis of the lacunar–canalicular network morphology and its relation to the strains experienced by osteocytes in situ as predicted by case-specific finite element analysis. *Biomech Model Mechanobiol.* 2015;14(2):267–82.
58. Schneider P, Meier M, Wepf R, Müller R. Serial FIB/SEM imaging for quantitative 3D assessment of the osteocyte lacuno-canalicular network. *Bone.* 2011;49(2):304–11.